

Design of a Miniature Circularly Polarized Antenna Operating in Three Frequency Bands Using a Polarized Ferrite Material

Sarra Jemmeli¹, Thierry Monediere¹, Eric Arnaud¹, and Laure Huitema¹, *Member, IEEE*

Abstract—The purpose of this article is to show the strong potential of ferrite materials to improve antennas performances. Indeed, the combination of circular polarization with miniaturization and multiband frequency operation makes ferrites the ideal solution to optimize antenna's characteristics. In this work, the complete development of a miniature antenna having dimensions of $(\lambda_0/9.6) \times (\lambda_0/9.1) \times (\lambda_0/27.4)$ at 3.13 GHz, operating over three frequency bands, and having a circular polarization is detailed. The benefit of incorporating such ferrite materials within an antenna on the radiation efficiency, the impedance bandwidth, and the axial ratio is presented. The prototype measurement will validate this development and the simulation results.

Index Terms—Circular polarization, miniaturization, multiband frequency, saturated ferrite materials.

I. INTRODUCTION

DEVELOPING antennas with high performances is a real challenge in the modern wireless communication systems. Indeed, many military and space applications require miniature and multiband antennas with circular polarization, which can also be an interesting solution in commercial fields in order to avoid polarization losses caused by multiple paths. However, this circularly polarized wave radiation is difficult to achieve when this objective must be combined with the miniaturization of the devices and a multiband operation.

In the literature, many studies focused on developing single-feed antennas capable of operating over dual frequency bands and with a circular polarization [1], [2]. In fact, some methods for achieving circular polarization consist in modifying the structure of a patch by adding slots [1]–[3] or by truncating the corners [4]. In [1], the device presents a single-feed slotted patch structure loaded by stubs to reduce the frequency ratio of the two working bands. Dimensions of the radiating element are $(\lambda_0/2.5) \times (\lambda_0/2.5) \times (\lambda_0/43.7)$ at 1.227 GHz. Another circularly polarized design, studied in [2], has dimensions of $(\lambda_0/3.3) \times (\lambda_0/3.3) \times (\lambda_0/125)$ at 1.575 GHz and includes four asymmetric slits and truncating corners to improve the operating frequency bandwidth (BW). The association of a

dual frequency band operation with a circular polarization can also be achieved by adding multiple feeds or a feeding network [5], [6]. Indeed, a microstrip feeding network is combined with a crossed-slot feed for developing a circularly polarized stacked-patch antenna [5]. A dual-orthogonal feed with a 90° phase shift is also used for achieving a circular polarization radiation in [7]. However, these feeding methods require power dividers or hybrid couplers, which present losses and need a larger ground plane size to place this feeding network, which can also affect the polarization purity.

Performances are good but antennas dimensions are too large when the application requires the device to be miniature. Moreover, these papers present a dual-band operation, which is another limitation of devices presented previously. Only few papers studied the case of triband circularly polarized antennas [8], [9]. In [8], the proposed circularly polarized antenna consists of four T-shaped slits integrated in a central patch to generate two frequency bands at 1.3 and 3 GHz. The third band (1.98 GHz) is generated by another radiating element (ring), which surrounds the central patch and fed independently. The device presents a return loss with impedance BW of 1.23%, 1.3%, and 1% at 1.3, 1.98, and 3 GHz, respectively, and the antenna size is about $(\lambda_0/3.3) \times (\lambda_0/3.3) \times (\lambda_0/153.9)$ at the first working frequency. In another research [10], a triband circularly polarized square slot antenna is exhibited. Feeding the antenna through a dual monopole feed makes the device working in three large BWs: from 1.96 to 3.26, 3.61 to 6.98, and 7.87 to 11.24 GHz. Embedding crooked T- and F-shaped strips to the antenna configuration improved the CP quality of the second band, whereas the axial ratio (AR) remains higher than 3 dB on the other functional band. The concept of multistacked patches is introduced in [11] to induce the triple band operation (at 1.176, 1.227, and 1.575 GHz). The designed antenna is excited through a single probe feed soldered to the upper patch and the two other radiating elements are fed through electromagnetic coupling. To obtain the circular polarization behavior, the upper and the middle patch corners are truncated, a slit in the lower patch is added, and two symmetry I-slot in the middle radiating element are integrated. The device shows a good AR of 1.54, 0.68, and 0.59 dB at the working frequencies, respectively. The proposed antenna has dimensions of $(\lambda_0/3.8) \times (\lambda_0/3.8) \times (\lambda_0/53.1)$ at the first working frequency (1.176 GHz).

To simplify and miniaturize the antenna geometry while having good performances over three frequency bands, the idea followed in this article is to use a ferrite material as substrate.

Manuscript received July 22, 2020; revised December 4, 2020; accepted December 6, 2020. Date of publication December 24, 2020; date of current version August 4, 2021. (Corresponding author: Sarra Jemmeli.)

The authors are with the XLIM Research Institute, CNRS UMR 7252, University of Limoges, F-87000 Limoges, France (e-mail: sarra.jemmeli@xlim.fr).

Color versions of one or more figures in this article are available at <https://doi.org/10.1109/TAP.2020.3045756>.

Digital Object Identifier 10.1109/TAP.2020.3045756

0018-926X © 2020 IEEE. Personal use is permitted, but republication/redistribution requires IEEE permission. See <https://www.ieee.org/publications/rights/index.html> for more information.

Indeed, an eigenmode study of an open ferrite resonator is presented in [12] and the resonance frequencies of the modes within a ferrite circular patch antenna, computed from the cavity model, are plotted as a function of the applied magnetic field. This article clearly demonstrates that for a given bias field value, these circularly polarized modes [right-handed circular polarization (RHCP) and left-handed circular polarization (LHCP)] can resonate at different frequencies, suggesting that a circular polarization can be obtained on three different frequency bands. In fact, the intrinsic properties of ferrite materials (especially anisotropy and nonreciprocal behavior) allow the antenna to generate a circularly polarized radiation field even when the device is excited with a single probe. This principle has been exploited in [13] where the two first RHCP and LHCP resonances have been generated within a ferrite patch antenna. Moreover, ferrites are appropriate substrates to have miniaturized antennas since they have a permeability higher than 1 combined to a high permittivity (between 12 and 15 typically). Therefore, Andreou *et al.* [13] presented a dual-band antenna (RHCP and LHCP) with a good broadside circular polarization while being miniature (dimensions of $(\lambda_0/4.4) \times (\lambda_0/4.4) \times (\lambda_0/21.4)$ at 4.6 GHz without considering the ground plane and the magnets). In addition to reduce the overall dimensions of an antenna, the combination of magnetic and dielectric behavior allows the impedance BW of an antenna to be increased compared with a pure dielectric device [14], [15]. Numerous studies on ferrite antennas have been reported in the literature, but measurement results are seldom discussed. Mashhadi *et al.* [16] simulated a parasitically coupled stack antenna. The designed antenna includes two-layer dielectric–ferrite substrate with a circular radiating element excited by a proximity-coupled feed line. To enhance the impedance BW, four parasitic patches are added on the top of a dielectric superstrate fed through electromagnetic coupling. The antenna operates over a wide frequency range of 44% and the AR is lower than 3 dB along all the matched impedance BW, whereas the antenna dimensions at the center frequency 4.4 GHz are about $(\lambda_0/1.35) \times (\lambda_0/1.35) \times (\lambda_0/10)$. While the antenna presents great performances in terms of impedance BW and AR, neither the magnetostatic study, which takes into account the real magnetic field, nor the measurement results are presented.

In this article, the development of a miniature and circularly polarized patch antenna operating in three frequency bands is proposed. This device uses a ferrite substrate and is excited with a single probe feed. The dispersive behavior (frequency dependence) of the ferrite permeability is exploited, which implies that the antenna can simultaneously operate on its fundamental mode at three different frequencies.

It is the first time that such an antenna has been studied as a whole, that is to say with the following.

- 1) A miniaturized triple-band device radiating right and left circular polarizations and using ferrite material.
- 2) A complete magnetostatic study allowing to perfectly know the static magnetic field used to polarize the ferrite. This accurate knowledge is essential before any realization and measurement.

- 3) A prototype measured and polarized with permanent magnets, i.e., in a configuration suitable for a practical use.

Section II is dedicated to a theoretical study of a patch antenna made of a saturated ferrite material. Indeed, a modal analysis of a ferrite circular patch antenna based on Pozar's studies [12] is presented. Section III details the modeling of the antenna and correlates it to the results presented in Section II. This section considers a ferrite antenna where an ideal magnetic polarization is used, i.e., the internal magnetic field (H_i) is homogenous. The antenna performances are evaluated through simulations using the software CST Microwave Studio [17]. Then, a magnetostatic study of the structure with real magnets (above and below the patch) is made in order to characterize with a good accuracy the internal magnetic field in the ferrite (amplitude, homogeneity, and so on). This magnetostatic simulation is also performed in order to choose dimensions and properties of magnets to be integrated. The final step associates the previous magnetostatic study with an electromagnetic simulation to determine the influence of the nonhomogeneous field on the antenna parameters in the real case, i.e., it allows the consideration of the real dc magnetic field within the structure. The different radiation characteristics such as the radiation efficiency (η_{rad}), the AR, the reflection coefficient ($|S_{11}|$), and the impedance BW are analyzed. Section IV deals with the presentation of the prototype and its measurement. This section validates our development since a miniature antenna offering a circular polarization on three frequency bands is exhibited. The relevance of this study is finally demonstrated by comparing the performances of this antenna with other kind of antennas presented in the literature in terms of dimensions, ARs, and frequency bands.

II. INFLUENCE OF FERRITE MATERIALS PROPRIETIES ON ANTENNA'S PERFORMANCES

A. Saturated Ferrite Materials Characteristics

The most significant parameter of ferrites is their permeability tensor. It describes their nonreciprocal behavior when they are biased with a continuous (dc) magnetic field. When the dc magnetic field is strong enough to saturate the ferrite, its permeability tensor is described by (1) called Polder tensor [18]

$$[\mu_r(\omega)] = \begin{bmatrix} \mu & -j\kappa & 0 \\ j\kappa & \mu & 0 \\ 0 & 0 & 1 \end{bmatrix} \quad (1)$$

where the elements of the permeability tensor are given by

$$\begin{aligned} \mu &= 1 + \frac{\omega_m \omega_0}{\omega_0^2 - \omega^2} = \mu' - j\mu'' \\ \kappa &= \frac{\omega_m \omega}{\omega_0^2 - \omega^2} = \kappa' - j\kappa'' \end{aligned} \quad (2)$$

With $\omega = 2\pi f$, ω_m the gyrotropic frequency defined by $\omega_m = \gamma \mu_0 M_s$, and ω_0 the Larmor frequency given by

$$\omega_0 = \gamma \mu_0 H_i + j\omega\alpha.$$

The permeability tensor elements depend on the frequency f , the internal magnetic field of the ferrite H_i , and the saturation

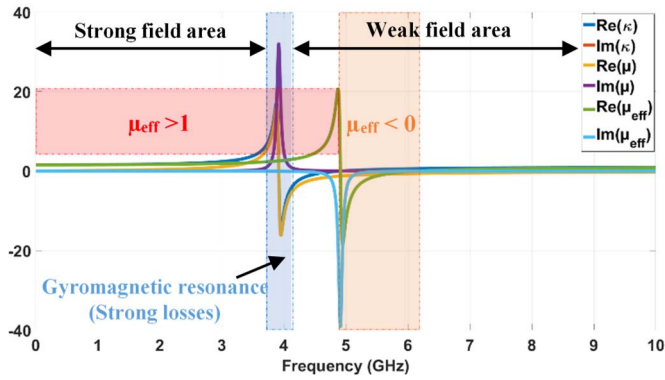


Fig. 1. Polder's parameters versus frequency for Y39 ferrite with $H_i = 1400\text{Oe}$.

magnetization M_s [18]. In addition, the Polder tensor takes into account the magnetic losses which are modeled by the damping factor $\alpha = (\gamma \Delta H)/(2fd)$, where ΔH is the ferrite linewidth.

Another important parameter that defines the operating zones of ferrite antennas is the effective permeability, which is expressed by the following equation:

$$\mu_{eff} = \frac{\mu^2 - \kappa^2}{\mu}. \quad (3)$$

The evolution of the Polder tensor elements as a function of the frequency (Fig. 1) shows that two areas can be distinguished: the strong field area and the weak field area. The strong field area occurs when the operating frequency is lower than the gyromagnetic resonance, which takes place when the precession frequency reaches the Larmor frequency, while the weak field area is for frequencies higher than this resonance. Around the gyromagnetic resonance, magnetic losses are too high for an antenna to operate. Therefore, the proposed antenna will operate outside this resonance and will be optimized for having its working modes both in the weak and in the strong field zones in order to provide a multiband operation. In the strong field area (Fig. 1), ferrite materials show a high permeability and permittivity while having low losses, which are desirable to miniaturize the antenna's dimensions.

The ability to use ferrites for antennas development has been theoretically addressed by Pozar in [12]. He showed the presence of resonant modes by considering a circular patch antenna as a ferrite resonator. However, this study was only theoretical and the matching of the modes was not studied.

In this article, the modal analysis presented by Pozar will be applied to a concrete case where the objectives will be driven by demonstrating the proof of concept of a multiband ferrite antenna. For that, we will start from the modal analysis of a circular ferrite resonator, which will be presented in Section III.

B. Eigen Mode Approach of Saturated Ferrite Materials in an Antenna

Without applying any external bias field, magnetic materials have the same characteristics as conventional dielectrics.

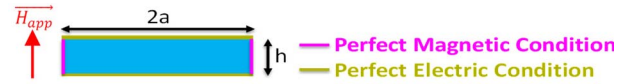


Fig. 2. Boundary conditions within the circular cavity model of radius a .

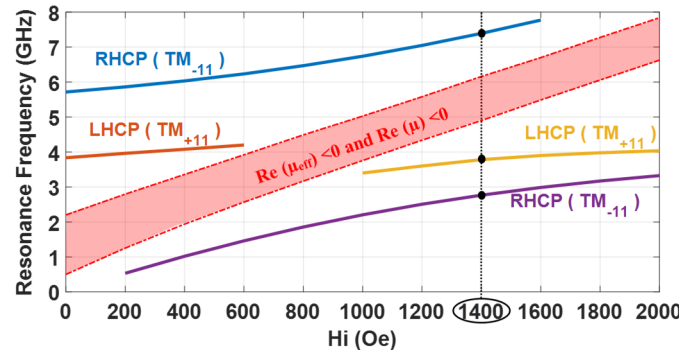


Fig. 3. Evolution of resonance frequencies versus the internal magnetic field strength for $a = 5 \text{ mm}$, with $4\pi M_s = 800 \text{ Gauss}$ and $\epsilon_r = 14.4$.

Therefore, the radiation field generated by a patch antenna excited with only one feeding probe has a linear polarization. However, under a dc magnetization, the radiated polarization will be changed from linear to circular [thanks to the tensor permeability described by (1)]. In addition, for a given applied magnetic field, the antenna can present several circular polarizations at different frequencies, i.e., RHCP and LHCP which implies that the antenna operates over several frequency bands.

To further understand this phenomenon, a circular patch antenna is considered as a circular cavity model of radius a . By assuming that the cavity walls are perfect electric walls on its bottom and top faces and a perfect magnetic wall on its lateral face (see Fig. 2), the wave equation for the fundamental TM_{11} modes can be written as follows [12]:

$$\frac{\partial^2 E_z}{\partial \rho^2} + \frac{1}{\rho} \frac{\partial E_z}{\partial \rho} + \frac{1}{\rho^2} \frac{\partial^2 E_z}{\partial \phi^2} + k^2 E_z = 0. \quad (4)$$

\vec{H}_{app} is the applied magnet field produced by the permanent magnets.

Considering these boundary conditions, the resonance frequencies of the cavity eigenmodes can be deduced by solving the following equation:

$$J'_1(ka) + n \times \frac{\kappa}{ka\mu} J_1(ka) = 0. \quad (5)$$

With J_1 the Bessel function, J'_1 the derivative of the Bessel function, and k the propagation constant given by the following equation:

$$k = \omega \sqrt{\epsilon \mu_{eff}}. \quad (6)$$

The above equations were implemented in a MATLAB [19] code to numerically solve (5). Fig. 3 shows the resonance frequencies of this modal study, plotted versus the internal magnetic field. In Fig. 3, two areas can be distinguished, below and above the region where real parts of μ and μ_{eff} are negative. In each of these two areas, two modes RHCP

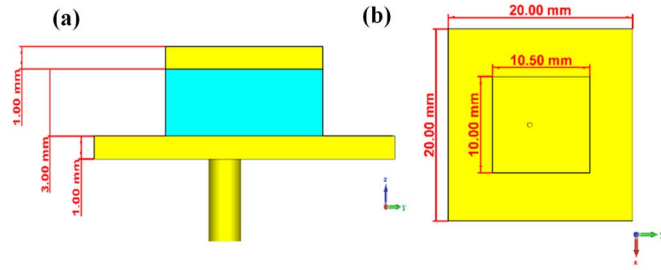


Fig. 4. (a) Side and (b) front views of the designed antenna.

($n = -1$) and LHCP ($n = +1$) appear implying that a multi-band operation can be achieved if the antenna is successfully matched on these modes. It appears in [12] that H_ϕ and H_r have the same amplitude with a phase quadrature which means that we have a circular polarization.

Solving (5) shows that, for a chosen magnetic field of 1400Oe, three RHCP and LHCP modes appear in the strong and the weak field area. The ferrite material properties and the internal magnetic field strength specify the working frequencies of these modes which mean that the three working bands cannot be tuned separately.

RHCP and LHCP polarities could be switched by reversing the direction of the applied static magnetic field. In the study detailed in this paragraph, the antenna under investigation presented a circular shape since the analytical equations are easier to implement with Bessel's equations. However, the next antenna modeled, realized, and measured will be a rectangular patch. There are two main reasons for that.

- 1) First, the antenna will be easier to manufacture.
- 2) Second, the use of a rectangular structure gives more degrees of freedom (x, y) on the position of the feeding probe. This is very useful to optimize the matching and the AR for each working frequency band.

Since the aiming antenna is miniature, a matching criterion of -6 dB is chosen.

III. SIMULATIONS

A. Ideal Case Study: Homogenous Biasing Field

The geometry of the designed antenna is depicted in Fig. 4. The device is a rectangular patch antenna on a ferrite material substrate Y39 (Yttrium–Aluminum) and fed through a single coaxial probe. The rectangular patch antenna dimensions are $l = 10$ mm, $w = 10.5$ mm, and $h = 4$ mm, i.e., close to the diameter of the circular antenna analytically studied in paragraph II.

The Y39 material presents a relative permittivity $\epsilon_r = 14.4$ with an accuracy of 5%, a dielectric loss tangent $\tan \delta = 2 \times 10^{-4}$, a saturation magnetization $4\pi M_s = 800$ Gauss, and an effective resonance linewidth $\Delta H_{eff} = 4$ Oe. This parameter (ΔH_{eff}) allows to take into account magnetic losses in the computation. In this case, the ferrite substrate is biased with a homogenous magnetic field of 1400Oe, chosen in order to obtain three resonance frequencies around 3, 4, and 7 GHz (deduced from the study presented in Fig. 3).

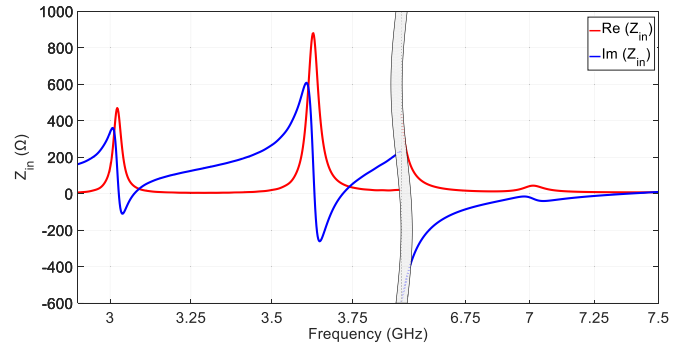


Fig. 5. Real and imaginary part of the input impedance.

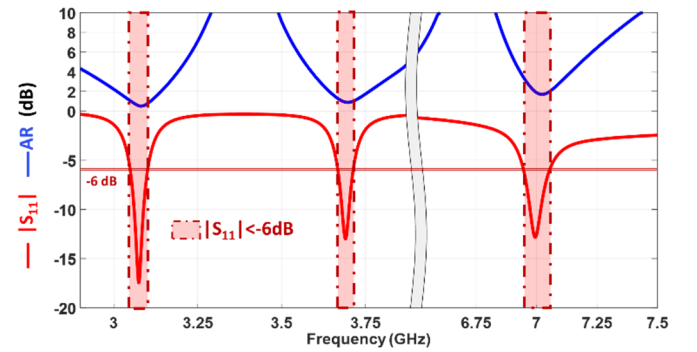


Fig. 6. $|S_{11}|$ parameter and AR of the ferrite-based patch antenna considering a uniform $H_i = 1400$ Oe.

This antenna is simulated in both strong field and weak field areas. Fig. 5 plots the frequency dependence of the input impedance Z_{in} . This figure highlights resonance frequencies of the structure that can be compared with the previous modal study presented in Fig. 3. As expected, three modes exist within the structure with a small frequency shift compared with Fig. 3, which can be explained by the rectangular structure considered in this case.

The position of the feeding probe is optimized in order to match the antenna on the three $TM_{\pm 11}$ modes within the structure. Dimensions of the patch (l, w) are also optimized particularly to improve the AR. Fig. 6 is showing the $|S_{11}|$ parameter plotted versus the frequency for both strong and weak fields. According to this figure, in the strong field area, two counter-rotating modes TM_{-11} and TM_{+11} are excited within the antenna. The first one is an RHCP and appears at 3.07 GHz and the second mode is an LHCP at 3.69 GHz. The $|S_{11}|$ plot shows that it is lower than -6 dB (the fixed criterion) over a frequency range of 60 MHz ($BW = 2\%$) for the first working band (RHCP) and of 40 MHz ($BW = 1.1\%$) for the second band (LHCP). These narrow BWs are explained by the fact that the antenna is miniature for these frequencies. In fact, the device dimensions are $(\lambda_0/9.8) \times (\lambda_0/9.3) \times (\lambda_0/24.4)$ on the first RHCP mode and about $(\lambda_0/8.1) \times (\lambda_0/7.7) \times (\lambda_0/20.3)$ on the LHCP mode. For the weak field area, a second RHCP mode appears at 7 GHz. The antenna is well matched with a $|S_{11}| < -6$ dB on a BW of 1.5%. For this frequency, the antenna dimensions are about $(\lambda_0/4.3) \times (\lambda_0/4) \times (\lambda_0/10.6)$.

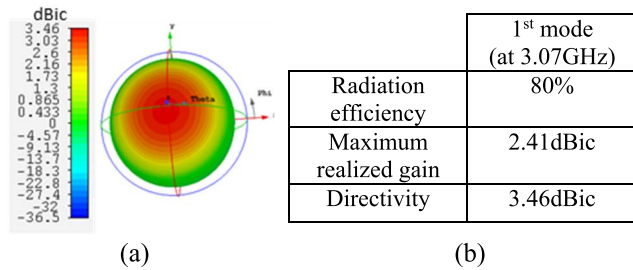


Fig. 7. (a) 3-D radiation pattern for the first RHCP mode at 3.07 GHz (radiation patterns are the same on the two other frequency bands) and (b) radiation characteristics of the first mode.

In order to evaluate the circular polarization quality of this antenna, the boresight AR is also plotted in Fig. 6. Thanks to the optimization of dimensions, the feeding probe position, and the choice of the applied static magnetic field, it appears that the boresight AR is very low for the three matching bands. Indeed, it is lower than 1, 1.26, and 3.2 dB for the three bands, respectively. For the third band, it is not as low as for the two first frequency bands since the height of the ferrite is quite high at this frequency.

For a better description of the radiation properties of the studied antenna, the 3-D radiation pattern of the first mode is shown at 3.07 GHz in Fig. 7(a). The radiation pattern has a boresight direction as a classical patch antenna and it has the same shape for the two other working frequencies. The first RHCP mode radiation characteristics are reported in Fig. 7(b).

The antenna radiates more than 70% of the accepted power on its two first operating bands, i.e., where $|S_{11}|$ is lower than -6 dB. More particularly, the radiation efficiency reaches 80% at the central frequency of the first matching band, which is a good value considering that the antenna is miniature at this frequency. For the third mode, the radiation efficiency is higher than 80%.

Under a uniform “ideal” magnetic bias field of 1400Oe, the designed antenna presents three circularly polarized modes and the device is miniature over the strong field area. The next step consists in simulating the antenna performances in the case of a “real” magnetic polarization. Indeed, the external magnetic field is provided by two permanent magnets. The geometry and characteristics of magnets have to be adjusted to provide an internal magnetic field of 1400Oe in order to obtain performances close to the ones presented in this paragraph. Therefore, next paragraphs will present the magnetostatic simulation and its combination with the electromagnetic simulations.

B. Magnetostatic Study

In order to characterize the internal magnetic field behavior into the ferrite substrate, we proceed to a magnetostatic study for the antenna structure designed above. The ferrite is magnetized using two commercial permanent magnets [20]. The upper one is Samarium Cobalt ($B_{r1} = 1.1$ T, $t_1 = 2$ mm, $\mu_{r1} = 1.15$) having the same surface as the radiating element ($l = 10$ mm, $w = 10.5$ mm). The second one is cylindrical with 9 mm of radius. This magnet is Neodymium ($B_{r2} = 1.35$ T, $t_2 = 3.6$ mm, $\mu_{r2} = 1.2$)

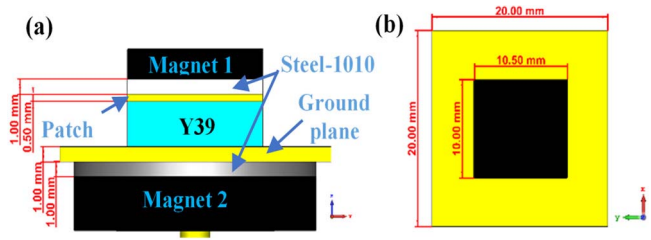


Fig. 8. (a) Side and (b) front views of the final designed antenna.

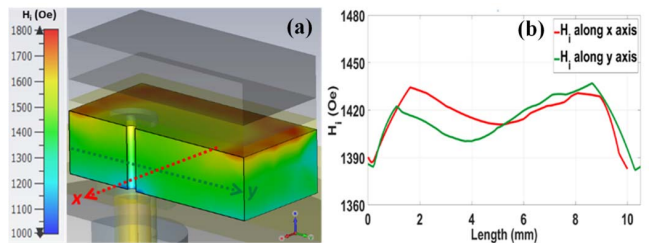


Fig. 9. (a) 3-D internal magnetic field distribution. (b) Evolution of the internal magnetic field in the middle of the ferrite material along x - and y -axes.

placed under the ground plane. Two Steel-1010 plates are added to homogenize the internal field within the ferrite. The first Steel plate is placed between the radiating element and the upper magnet and the second one between the ground plane and the lower magnet. Other manufacturing constraints are introduced (soldering, the magnet hole diameter, and so on) to model the real operation of the patch antenna. The device elements dimensions (Steel plates, the patch, and the ground plane thickness) are then adjusted to keep an internal field of 1400Oe. The final design of the antenna is given in Fig. 8.

The magnetostatic fields are calculated in 3-D within the whole structure. The internal field distribution is extracted and Fig. 9(a) presents an example of 3-D cartography of the dc magnetic field. According to this figure, the internal magnetic field is quite uniform in the middle of the ferrite substrate. The evolution of H_i along the x - and y -axes in the middle of the ferrite material is evaluated in Fig. 9(b). On these graphs, we notice that the field varies between 1380Oe and 1430Oe, i.e., close to the target value of 1400Oe. Since the most difficult step in the current design is to maintain a uniform magnetic field throughout the substrate, the idea was to homogenize as much as possible the internal magnetic field in the middle of the ferrite substrate. However, this involved an increasing of the field on the top of the substrate. In addition, drilling the ferrite and the lower magnet to insert the feeding probe led to the decreasing of the internal field near the hole. In order to overcome the inhomogeneity problems that could affect the device operation, the antenna parameters were adjusted.

The next step is to simulate the electromagnetic performances of this antenna structure by integrating these magnetostatic results, i.e., simulating the antenna in the real case. The antenna behavior, under the influence of a real biasing field, will be investigated.

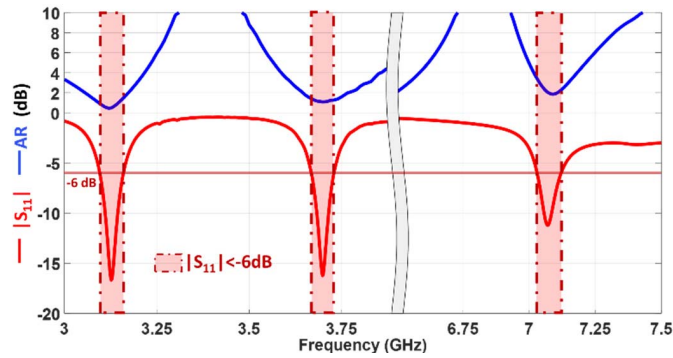


Fig. 10. $|S_{11}|$ parameter and AR versus frequency for inhomogeneous H_i .

C. Magnetostatic-Electromagnetic Cosimulation of the Antenna

We combine the previous magnetostatic analysis with an electromagnetic study to simulate the patch antenna with the real magnets, i.e., when the internal magnetic field is not completely homogeneous but the one from the previous magnetostatic study.

Fig. 10 shows the evolution of the $|S_{11}|$ parameter and the AR, respectively.

Compared with the previous ideal case, there is a slight frequency shift, since operating bands are centered at 3.13 GHz for the first RHCP mode, 3.7 GHz for the LHCP mode, and 7.1 GHz for the second RHCP mode.

The antenna presents a good boresight circular polarization, since it is lower than 1.5, 1.56, and 3.4 dB for the three matching bands, considering a $|S_{11}| < -6$ dB as a criterion (this criterion is usual for miniature antennas).

The radiation pattern shape remains the same as the one of a classical patch and already presented in Fig. 7(a). Radiation efficiencies are very close to the ideal case, i.e., higher than 70% at 3.13 and 3.7 GHz and higher than 80% at 7.1 GHz.

The simulated results of the designed antenna for a biasing magnetic field generated by two permanent magnets show a good concordance with those obtained when the applied magnetic field is homogenous. That means that the magnets have been correctly chosen in terms of remanent flux density (B_{r1} and B_{r2}) and dimensions. Finally, the antenna operates over three frequency bands in the strong and the weak field areas, with a circular polarization while being miniature. Since the antenna is compact in the strong field area, a compromise has been made in order to optimize the device performances in this area which explain the degradation of the antenna characteristics on the third mode where the antenna is not miniature. The next step consists in the validation of this development by the realization and the measurement of a prototype.

IV. MEASUREMENT

Once the antenna behavior has been simulated, the next step is to validate the performances with a prototype measurement [see Fig. 11(a) and (b)]. The different antenna elements are aligned and adjusted by a support structure made of Rohacell

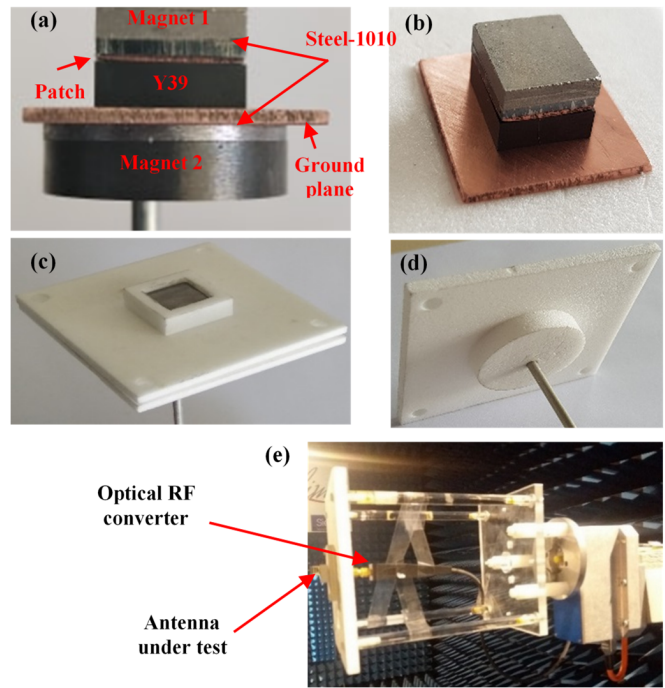


Fig. 11. (a) Side and (b) front views of the prototype. (c) Top and (d) bottom views of the prototype with Rohacell supporting structure. (e) Antenna under measurement.

material, as shown in Fig. 11(c) and (d). The antenna is measured in the anechoic chamber and an optical RF converter is used to reduce any perturbations of the measurement cable [Fig. 11(e)]. However, this measurement device remains large compared with the very low dimensions of the ground plane. This implies that a parasitic current flows over this device and creates disturbances on the antenna radiation. However, the measurement with this device remains better than with a classical RF cable since it is ended by an optical fiber, i.e., that avoids the surface current on the cable [21]. Indeed, the RF measurement cable involves a strong disturbance of the antenna's radiation and especially when the antenna (including the ground plane) is miniature.

The $|S_{11}|$ parameter of the antenna is measured and plotted in Fig. 12. The three operating frequency bands are at 3.3, 3.9, and 7.54 GHz, respectively. Therefore, there is a frequency shift of almost 6% for the three central frequencies with the simulation, which can be explained by the fact that the permittivity of the ferrite material is given with an accuracy of 5%.

On the first mode, $|S_{11}|$ is lower than -6 dB on a frequency range of 110 MHz, corresponding to an impedance BW of 3.3%. The frequency range of the second mode also equals 110 MHz, which corresponds to an impedance BW of 2.8%. For the weak field operation, the impedance BW is about 1.5%, corresponding to 110 MHz around 7.54 GHz.

According to the AR plot reported in Fig. 12, the antenna presents a good boresight circular polarization, since it is lower than 2.6 dB for the two first working bands and 3.9 dB for the third matching bands (< 3 dB at 7.54 GHz), i.e., where the $|S_{11}|$ parameter is lower than -6 dB.

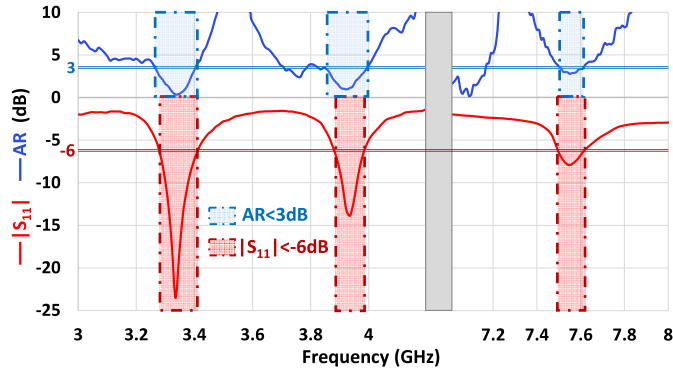


Fig. 12. $|S_{11}|$ parameter and AR of the measured antenna.

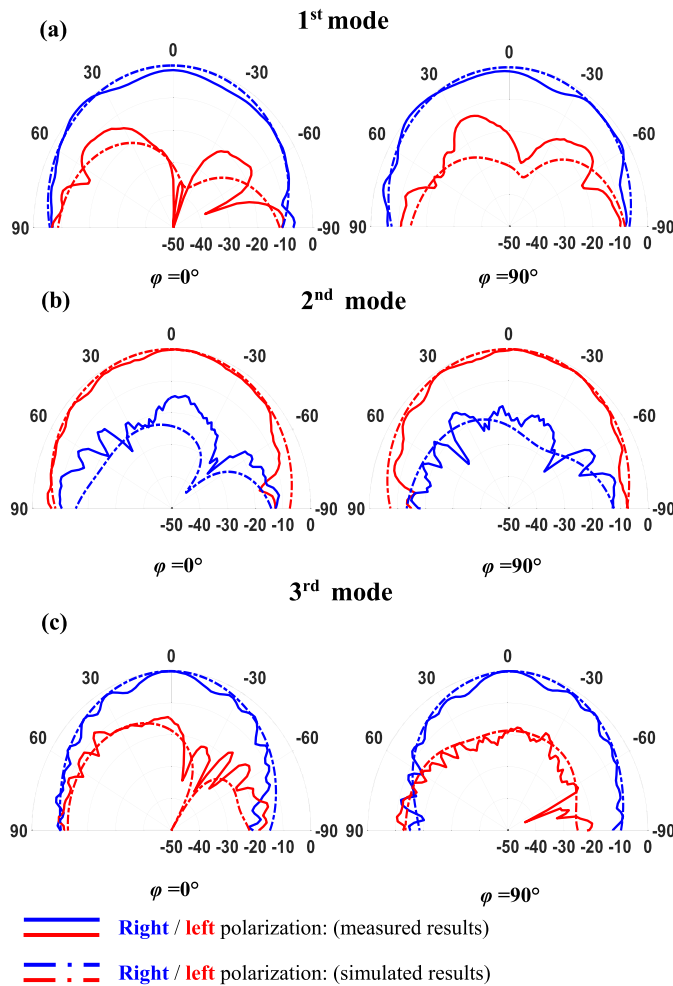


Fig. 13. Normalized circularly polarized radiation patterns at (a) 3.3, (b) 3.9, and (c) 7.54 GHz for the cutting planes $\varphi = 0^\circ$ and $\varphi = 90^\circ$.

Fig. 13 shows the simulated and measured normalized right and left polarization at the frequencies 3.3, 3.9, and 7.54 GHz for two cutting planes ($\varphi = 0^\circ$ and $\varphi = 90^\circ$). The measured radiation patterns are basically identical to the simulated ones validating the polarity of each mode. It can be seen that the first and the third modes present an RHCP and the second one has an LHCP.

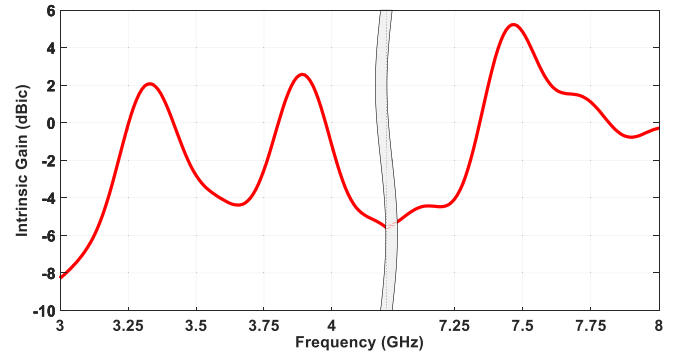


Fig. 14. Measured intrinsic gain versus the frequency.

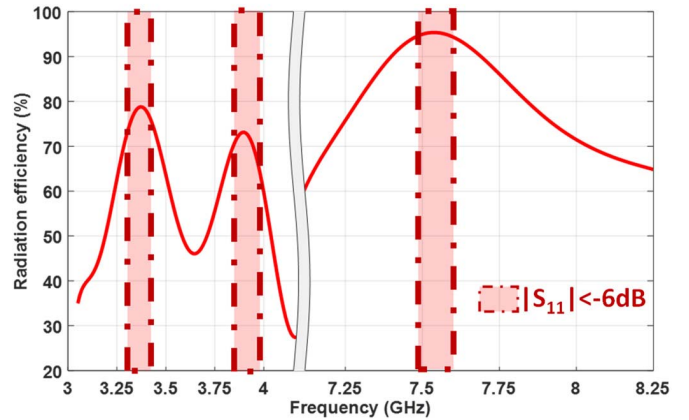


Fig. 15. Measured radiation efficiency over the strong field and weak field area.

The measured intrinsic gain versus the frequency is reported in Fig. 14. It can be observed that the antenna can attain a gain of 1.8, 2.6, and 3.7 dBic at the three center frequencies.

Moreover, the radiation efficiency on the strong and weak field region is illustrated in Fig. 15.

We can notice that the antenna radiates 79% of the accepted power on the first RHCP mode, which is a good value considering that the antenna is miniature at these frequencies. This radiation efficiency is higher than 75% on the LHCP mode, which is a lower value due to the fact that 3.7 GHz is closer to the gyromagnetic resonance area presenting high magnetic losses. For the second RHCP mode, i.e., in the weak field region, the radiation efficiency is higher than 95%. For this mode, the antenna presents a better radiation efficiency because the device is not as miniature as on the strong field area modes.

Simulations are, therefore, validated and these performances can be compared with results existing in the literature in Table I. The antennas dimensions are calculated considering the radius of the smallest sphere containing the device (noted r in Fig. 16) [22]. Therefore, this dimension takes into account all the elements that constitute the overall radiating system, in this case the magnets as well as the ground plane. An electrically small antenna is defined as an antenna with the dimension r is lower than $\lambda_0/2\pi$ [22].

According to the comparative table reported above, it can be deduced that the proposed antenna operates over three

TABLE I

COMPARISON BETWEEN THE PROPOSED AND SOME PUBLISHED ANTENNA

Structure	Working frequencies (f_w)	AR at f_w	η_{rad} at f_w	Dimension r at the first frequency f_w
Proposed	3.3GHz 3.9GHz 7.54GHz	0.4dB 1dB 2.8dB	79% 75% 95%	$\frac{\lambda_0}{6.5}$
[8]	1.3GHz 1.98GHz 3GHz	2.9dB 2dB 1.9dB	N/A	$\frac{\lambda_0}{3.8}$
[9]	2.04GHz 2.44GHz 3.44GHz	0.7dB 1.7dB 1.2dB	N/A	N/A
[1]	1.227GHz 1.575GHz	1dB 0.4dB	98% 98%	$\frac{\lambda_0}{3.5}$
[13]	4.6GHz 5.31GHz	4.2dB 2.6dB	97% 98%	$\frac{\lambda_0}{2.8}$

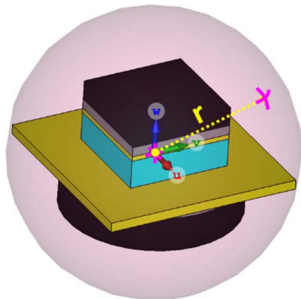


Fig. 16. Sphere circumscribing the antenna.

frequency bands and presents a lower AR and good radiation efficiencies at the center working frequencies (at 3.3, 3.7, and 7.54 GHz). Moreover, the device is much more compact than the reported designs with an r dimension equal to 14.1 mm corresponding to $\lambda_0/6.5$ at 3.3 GHz, the first working frequency, i.e., lower than $\lambda_0/2\pi$.

V. CONCLUSION

The purpose of this article was to demonstrate, for the first time, a miniature circularly polarized triband antenna using a ferrite material. Indeed, the goal was to take advantage of the magnetic properties of ferrite materials to design a patch antenna using only one excitation probe and capable of generating circular polarization. Modal study of such a structure, considered as a resonator, shows that the dispersive nature of the ferrite permeability implies that the fundamental mode appears at three different frequencies. The exploitation of this phenomenon has thus enabled the antenna to operate over

several frequency bands while radiating circular polarization, without the need to add a feeding network.

Moreover, ferrites are appropriate substrates to have miniaturized antennas since they have a high permittivity combined to an effective permeability higher than 1. The designed antenna is, therefore, miniature ($\lambda_0/6.5$) at 3.3 GHz and has circular polarization on three frequency bands. The antenna has been manufactured and the measured performances are convincing since the demonstration of a triband ferrite antenna has been done with very good AR considering that the antenna is miniature. The comparison of the performances obtained with those in the literature shows that the use of ferrite materials is very interesting in the field of miniature antennas.

ACKNOWLEDGMENT

This work has been carried out in the framework of a joint laboratory INOGYRO between the SME Inoveos and the XLIM Laboratory (<https://inogyro.xlim.fr/>).

REFERENCES

- [1] A. A. Heidari, M. Heyrani, and M. Nakhkash, "A dual-band circularly polarized stub loaded microstrip patch antenna for GPS applications," *Prog. Electromagn. Res.*, vol. 92, pp. 195–208, 2009.
- [2] K. S. Rao, D. R. Jahagirdar, and D. Ramakrishna, "Compact broadband asymmetric slit circularly polarized microstrip patch antenna for GPS and GLONASS applications," in *Proc. IEEE Int. Conf. Antenna Innov. Mod. Technol. Ground, Aircr. Satell. Appl. (iAIM)*, Nov. 2017, pp. 1–3.
- [3] K.-P. Yang and K.-L. Wong, "Dual-band circularly-polarized square microstrip antenna," *IEEE Trans. Antennas Propag.*, vol. 49, no. 3, pp. 377–382, Mar. 2001.
- [4] Z. N. Chen, X. Qing, and H. L. Chung, "A universal UHF RFID reader antenna," *IEEE Trans. Microw. Theory Techn.*, vol. 57, no. 5, pp. 1275–1282, May 2009.
- [5] D. M. Pozar and S. M. Duffy, "A dual-band circularly polarized aperture-coupled stacked microstrip antenna for global positioning satellite," *IEEE Trans. Antennas Propag.*, vol. 45, no. 11, pp. 1618–1625, Nov. 1997.
- [6] F. Bilotti and C. Vegni, "Design of high-performing microstrip receiving GPS antennas with multiple feeds," *IEEE Antennas Wireless Propag. Lett.*, vol. 9, pp. 248–251, May 2010.
- [7] F. Fezai *et al.*, "Low-profile dual-band circularly polarized microstrip antenna for GNSS applications," in *Proc. 9th Eur. Conf. Antennas Propag. (EuCAP)*, Lisbon, Portugal, Apr. 2015, pp. 1–4.
- [8] Y. Jie, L. Chunlan, and S. Juhong, "Design of a compact multi-band circularly-polarized microstrip antenna," in *Proc. Int. Symp. Antennas Propag.*, Nanjing, China, Oct. 2013, pp. 561–564.
- [9] Q. Liu and G. Han, "A novel tri-band circular polarization antenna," in *Proc. Cross Strait Quad-Regional Radio Sci. Wireless Technol. Conf. (CSQRWC)*, Taiyuan, China, 2019, pp. 1–2.
- [10] S. A. Rezaeieh and M. Kartal, "A new triple band circularly polarized square slot antenna design with crooked T and F-shape strips for wireless applications," *Prog. Electromagn. Res.*, vol. 121, pp. 1–18, 2011.
- [11] O. P. Falade, M. U. Rehman, Y. Gao, X. Chen, and C. G. Parini, "Single feed stacked patch circular polarized antenna for triple band GPS receivers," *IEEE Trans. Antennas Propag.*, vol. 60, no. 10, pp. 4479–4484, Oct. 2012.
- [12] D. M. Pozar, "Radiation and scattering characteristics of microstrip antennas on normally biased ferrite substrates," *IEEE Trans. Antennas Propag.*, vol. 40, no. 9, pp. 1084–1092, Sep. 1992.
- [13] E. Andreou, T. Zervos, A. A. Alexandridis, and G. Fikioris, "Magneto-dielectric materials in antenna design: Exploring the potentials for reconfigurability," *IEEE Antennas Propag. Mag.*, vol. 61, no. 1, pp. 29–40, Feb. 2019.
- [14] R. C. Hansen and M. Burke, "Antennas with magneto-dielectrics," *Microw. Opt. Technol. Lett.*, vol. 26, no. 2, pp. 75–78, 2000.
- [15] L. Huitema, T. Reveyard, J.-L. Mattei, E. Arnaud, C. Decroze, and T. Monediere, "Frequency tunable antenna using a magneto-dielectric material for DVB-H application," *IEEE Trans. Antennas Propag.*, vol. 61, no. 9, pp. 4456–4466, Sep. 2013.

- [16] M. Mashhadi, N. Komjani, B. Rejaei, and J. Ghalibafan, "Ferrite-based wideband circularly polarized microstrip antenna design," *ETRI J.*, vol. 41, no. 3, pp. 289–297, 2019.
- [17] *CST Microwave Studio*. Accessed: Dec. 28, 2020. [Online]. Available: www.3ds.com
- [18] E. Arnaud, L. Huitema, R. Chantalat, A. Bellion, and T. Monediere, "Miniaturization of a circular polarized antenna using ferrite materials," in *Proc. 12th Eur. Conf. Antennas Propag. (EuCAP)*, London, U.K., 2018, pp. 1–5.
- [19] *Matlab*. Accessed: Dec. 28, 2020. [Online]. Available: www.fr.mathworks.com
- [20] Accessed: Dec. 28, 2020. [Online]. Available: http://cermag.co.uk/magnet_properties.html
- [21] L. Huitema, C. Delaveaud, and R. D'Errico, "Impedance and radiation measurement methodology for ultra miniature antennas," *IEEE Trans. Antennas Propag.*, vol. 62, no. 7, pp. 3463–3473, Jul. 2014.
- [22] H. Wheeler, "The radiansphere around a small antenna," *Proc. IRE*, vol. 47, no. 8, pp. 1325–1331, Aug. 1959.



Sarra Jemmeli received the master's degree in high-frequency electronics from the University of Limoges, Limoges, France, in 2018, where she is currently pursuing the Ph.D. degree within the RF systems axis of the Antennas and Signals Team, XLIM Laboratory.

Her research focuses on circularly polarized, miniature, and multiband antennas using ferrite materials.



Thierry Monediere was born in Tulle, France, in 1964. He received the Ph.D. degree from the IRCOM Laboratory, University of Limoges, Limoges, France, in 1990.

He is currently a Professor with the Antennas and Signals Team, XLIM Research Laboratory, University of Limoges. He develops his research activities in this laboratory and works on multifunction antennas, miniature antennas, antenna arrays, and also active antennas. He also studies gyromagnetic devices as ferrite circulators or isolators.



Eric Arnaud was born in France in 1970. He received the Diplôme D'Etudes Supérieures Spécialisées (DESS) and Ph.D. degrees in electronics and telecommunication from the University of Limoges, Limoges, France, in 1994 and 2010, respectively. He did his Ph.D. in circularly polarized EBG antennas.

From 1996 to 2001, he has been in charge of the Microwave part of Free-Electron Laser (L.U.R.E). Since 2001, he has been in charge of XLIM Laboratory's antenna test range. He participated in several research projects related to the design, development, and characterization of antennas. His research interests are mainly in the fields of circularly polarized EBG antennas, agile electromagnetic bandgap matrix antennas, and isoflux pattern antennas.



Laure Huitema (Member, IEEE) received the M.S. and Ph.D. degrees in telecommunications high frequencies and optics from the University of Limoges, Limoges, France, in 2008 and 2011, respectively.

From 2011 to 2012, she was a Post-Doctoral Research Fellow at the Atomic Energy Commission (CEA), Laboratory of Electronics and Information Technology (LETI), Grenoble, France. She is currently an Associate Professor with the Antennas and Signals Team within the RF systems axis of the

XLIM Research Institute, University of Limoges. More recently, she has been working on new components for their integration inside antennas. In this framework, she is the Project Leader of the H2020 European Project called MASTERS (http://www.unilim.fr/H2020_MASTERS/). She is currently the Director of the joint laboratory INOGYRO (<https://inogyro.xlim.fr/>) which brings together the XLIM Laboratory and the company Inoveos. Her research interests include reconfigurable antennas, dielectric resonator antennas, miniature antennas, multiband antennas, and circulators.

Dr. Huitema was a recipient of the Best Student Paper Award at the 2010 IEEE International Workshop on Antenna Technology and the Best Student Paper Award at the 2010 JCMM Conference. In 2020, she won the Bronze Medal of the French National Centre for Scientific Research (CNRS).